Electronic Supplementary Material (ESI) for ChemComm.

Mechanistic insights into sodium storage in hard carbon anodes using local structure probes

Joshua M. Stratford,[a] Phoebe K. Allan,[a,b,c] Oliver Pecher,[a] Philip A. Chater,[c] and Clare P. Grey.[a*]

[a] Department of Chemistry, University of Cambridge, Lensfield Road, Cambridge, CB2 1EW, U.K.

[b] Gonville and Caius College, Trinity Street, Cambridge, CB2 1TA, U.K.

[c] Diamond Light Source Ltd., Harwell Science and Innovation Campus, Didcot, OX11 0DE, U.K.

*Corresponding author: Professor Clare P. Grey, email: cpg27@cam.ac.uk

Supplementary Information

Experimental Methods

Except were otherwise stated, all experiments were performed under ambient conditions.

Electrode Preparation

Carbotron P(J) (Kureha Corporation) was mixed with 10% polyvinylidene fluoride-co-hexafluoropropylene (Kynar), to which one drop of dibutyl phthalate (Sigma-Aldrich) was added for every 10 mg of binder. Acetone (Sigma-Aldrich, anhydrous) was added, and the resultant slurry spread onto a glass substrate using a 300 μm doctor blade. After drying in air, the film was washed three times with diethyl ether (Sigma-Aldrich) and dried at 100 °C *in vacuo* prior to use.

PDF Analysis

Cells for PDF analysis were cycled at a rate of C/20 (based on the mass of carbon, with 1C corresponding to achieving a capacity of 300 mAhg^{-1} in one hour) to the point of interest on the electrochemical curve. The electrodes were recovered inside an argon atmosphere glovebox, washed with dimethylcarbonate (Sigma Aldrich, anhydrous, >99%) and immediately dried *in vacuo*. The electrode films were then individually ground and sealed into thin walled quartz capillary tubes (Hampton Research, OD=2 mm).

PDF data were collected at beamline I15-1 at Diamond Light Source using a wavelength of 0.163000 Å and a Perkin-Elmer flat panel detector. A CeO_2 standard was used to calibrate the sample geometry and the sample-to-detector distance. The data were converted to a function of intensity vs. Q using Data Analysis WorkbeNch (DAWN).[1] Standard corrections (background, Compton scattering, detector effects) were applied, and the data Fourier transformed (Qmax = 20.5 Å) to obtain G(r) using the software PDFGetX2.[2] Structural models were refined against PDF data using PDFGui.[3] Difference PDFs were calculated by subtracting the PDF for the pristine electrode from the PDFs of the electrodes at various stages of charge. Difference PDFs were r-averaged over termination ripples.

Solid-state NMR Spectroscopy

Operando solid-state NMR (ssNMR) measurements were performed using an in house designed electrochemical cell based upon a cylindrical capsule, details of which will be published at a later date. Cells were prepared in an argon atmosphere glove box (O_2, H_2O < 0.1 ppm) using metallic sodium (Sigma Aldrich, 99.9%) as an anode. The electrolyte was 1 M $NaPF_6$ (Alfa Aesar, ≥99%) in propylene carbonate (Sigma Aldrich, anhydrous), and the separator was borosilicate glass fibre (Whatman, GF/A). Electrochemical measurements were conducted on a Bio-Logic VSP battery cycler running EC-Lab® software version 10.40. Cells were cycled at a rate of C/20 (based on the mass of carbon, with 1C corresponding to achieving a capacity of 300 mAhg^{-1} in one hour) and held at 5 mV until the applied current dropped to C/100.

A Bruker Avance 300 MHz spectrometer with a ^{23}Na Larmor frequency of 79.39 MHz was fitted with a recently published, in house designed static probe with automatic tuning and matching capabilities (along with connections for an external battery cycler) and used for the measurements reported.[4] The electrochemical cell was aligned such that the electrodes were parallel to the applied field.

In order to maximise the signal-to-noise ratio for a time-restricted measurement, a one-pulse sequence was used. A 90° pulse corresponded to 3.5 μs at 200 W using an 11 mm diameter silver coil. 30000 transients were collected for each spectrum, using a recycle delay of 0.05 s (31 minutes per spectrum). The resonance circuit was recalibrated immediately prior to each acquisition by minimising the standing wave ratio of the forward and reflected power for a low power (0.01 W) continuous wave pulse.[4] The ^{23}Na signals were referenced using a 1M solution of NaCl at a shift of 0 ppm.[5] Spectra were Fourier transformed and individually phased using Bruker Topspin 3.2. Backgrounds were subtracted using fityk.[6]

Ex situ ^{23}Na MAS NMR measurements were performed using a Bruker Avance III 200 MHz spectrometer with a ^{23}Na Larmor frequency of 52.92 MHz and a Bruker Avance III 500 MHz spectrometer with a ^{23}Na Larmor frequency of 132.29 MHz. 1.3 mm zirconia rotors were spun at 60 kHz using a Bruker double resonance probehead. A MAS speed synchronised Hahn-echo pulse sequence with 90–180° pulses corresponding to 2–4 μs at 25 W was applied for the lower field measurements, at higher field, a one pulse sequence was applied; a recycle delay of 0.05 s was used. Spectra were referenced using NaCl powder at 7.21 ppm.[7]

Samples for *ex situ* MAS NMR investigations were prepared electrochemically; cells were cycled at a rate of C/20 (based on the mass of carbon, with 1C corresponding to achieving a capacity of 300 mAhg^{-1} in one hour) to the point of interest on the electrochemical curve. The electrodes were recovered inside an argon atmosphere glovebox (O_2, H_2O < 0.1 ppm), washed with dimethylcarbonate (Sigma Aldrich, anhydrous, >99%) and immediately dried *in vacuo*. The respective electrode films were then individually ground and packed into rotors immediately.

2. PDF data for electrodes at various states of charge

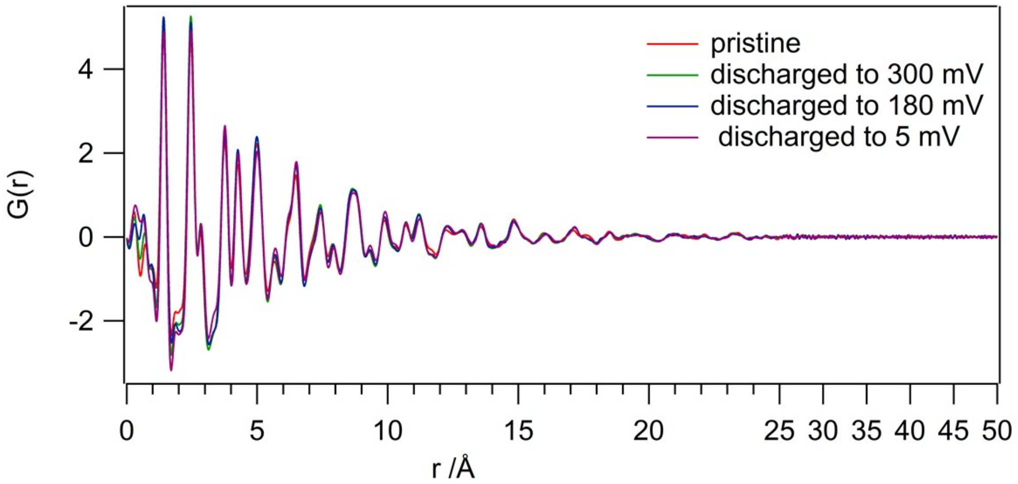

Figure S1: PDF data for electrodes at various stages of discharge. The red line corresponds to the pristine film, the green line to a sample discharged to 300 mV, the blue to 180 mV and the purple to 5 mV. Data were Fourier transformed using a Q_{max} of 20.5 Å.

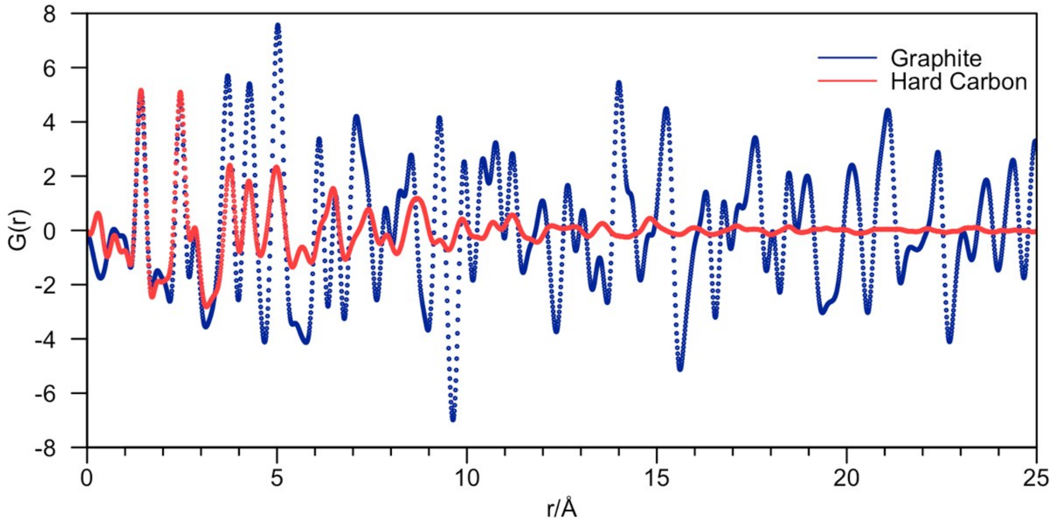

Figure S2: PDF data for the pristine hard carbon (red) and graphite (blue). Differences in peak intensity and position are evident for r > 3 Å.

3. PDF curvature calculations:

The experimentally observed interatomic distance, L, is related to the distance expected in a planar graphene sheet, G, and the radius of curvature, r, by:

$L = 2r\sin(G/2r))$ (Figure S3)

The positions of five peaks in the experimental PDF were compared to the distance expected in a model of a planar graphene sheet which has the first C-C distance at the experimentally-observed distance.

Table S1: Data used for radius of curvature calculations

Peak in experimental PDF /Å	Peak in model PDF /Å	Radius of curvature/Å
3.7604	3.7729	13.37
4.2602	4.2694	18.77
4.9942	5.0220	13.77
5.6727	5.7048	15.51
6.4770	6.5150	17.34
	Mean value	**15.76**
	Standard deviation:	**2.07**

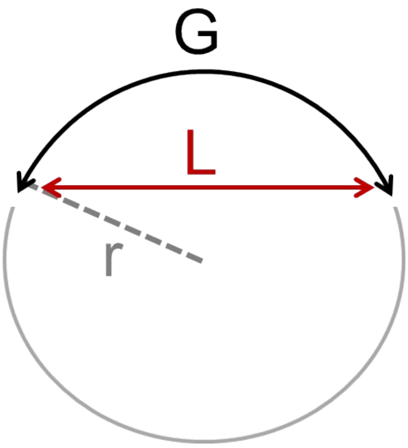

Figure S3: Diagram of the parameters used to calculate the average radius of curvature of the graphene fragments in the hard carbon.

4. PDF refinements

Real-space least-squares refinements against PDF data were performed in PDFGui.[3] A starting model of graphite was used. U_{33} parameters for all atoms were set to an initial value of 1, U_{11}, U_{22}, were set to 0.08. A spherical particle diameter of 20 Å was set. Unit cell parameters, phase scale factor, the spherical particle diameter, delta1 (low-r peak sharpening parameter) and the thermal parameters were all refined during refinements including low-r ($r < 5$ Å) data. For refinements not using low-r data, the value of delta1 was fixed to the value determined in refinements at low-r. For the comparison of the *a*-parameter, refinements were performed in the following r-ranges: 1 – 2 Å, 2 – 5 Å, 5 – 10 Å, 10 – 15 Å, 15 – 20 Å.

Table S2: Unit cell *a*-parameter values determined by performing real-space least-squares refinements in PDFGui.

Range (Å)	***a*-parameter / Å**
0-2	2.465
2-5	2.459
5-10	2.451
10-15	2.444
15-20	2.440

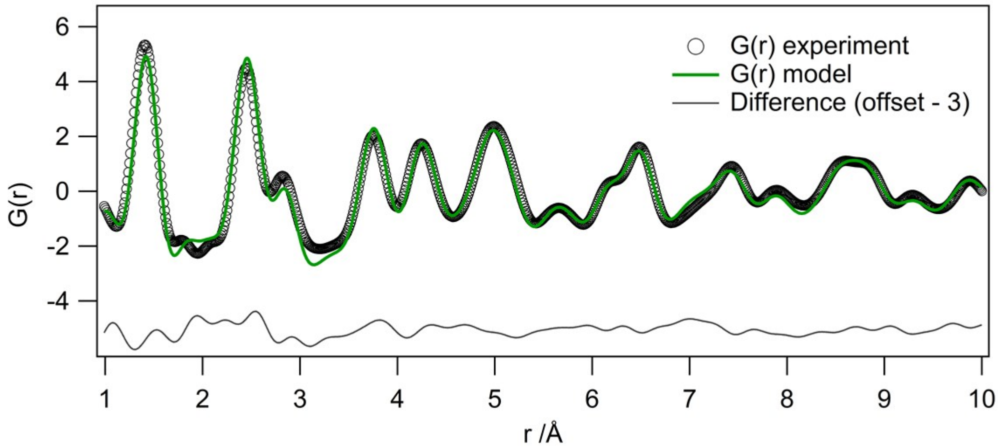

Figure S4: Real-space least-squares refinement of turbostratically disordered graphite against PDF data for the pristine electrode in the distance range 1 – 10 Å. Black circles show experimental data, the green line shows the calculated PDF for the model. The offset grey line shows the residual ($G(r)_{model} - G(r)_{expt}$).

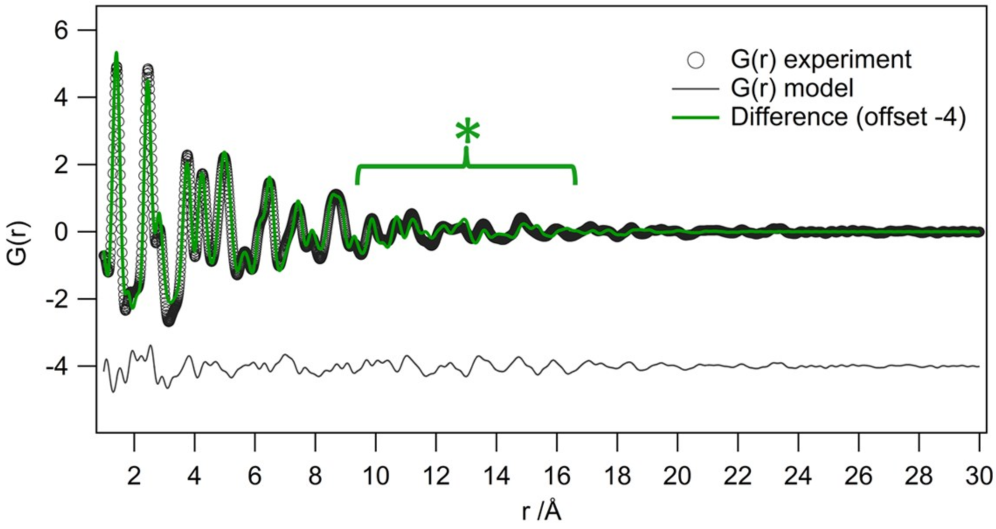

Figure S5: PDF calculated from the model refined against data in the distance range 1 – 10 Å extrapolated to the full range over which peaks are observed experimentally. The fit is particularly poor at r > 10 Å, indicating that planar graphene sheets are not sufficient to model the intermediate-range structure of the carbon. The region marked by * has a poor fit to the experimental data when using the parameters determined by a refinement at low-r. Black circles show experimental data, the green line shows the calculated PDF for the model. The offset grey line shows the residual ($G(r)_{model}$ – $G(r)_{expt}$).

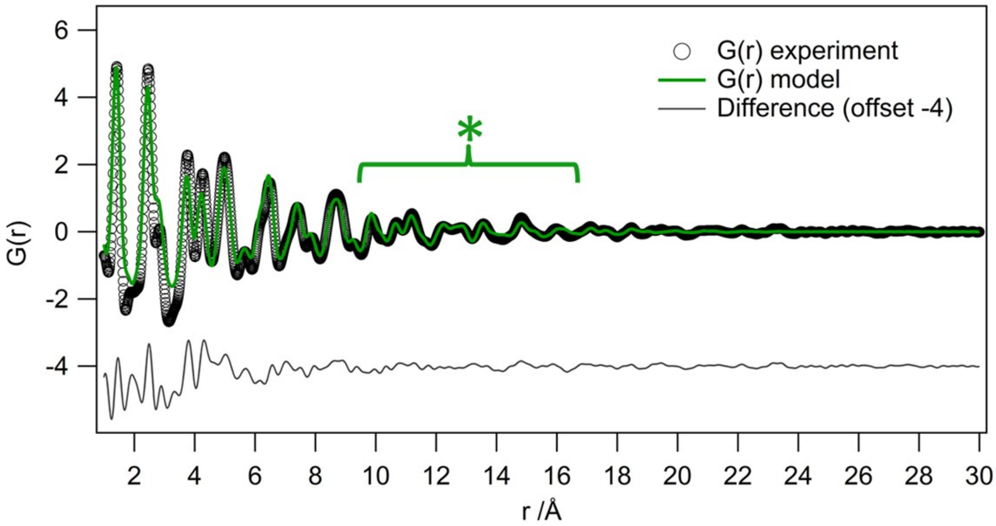

Figure S6: Refinement of turbostratically disordered graphite against PDF data using the parameters obtained from a refinement in the range of 10 – 20 Å. The fit to the model in the 10 – 20 Å range is much better than the model shown in Figure S3, but the fit to the low-r region is poorer. A decreased *a*-parameter implies sheet curvature. Increased thermal parameters are obtained for the refinement in this region, indicating increased disorder to the atom-atom correlations in this region, owing to the range of distances possible due to the curvature of the sheets and through the termination of fragments. Black circles show experimental data, the green line shows the calculated PDF for the model. The offset grey line shows the residual ($G(r)_{model} - G(r)_{expt}$).

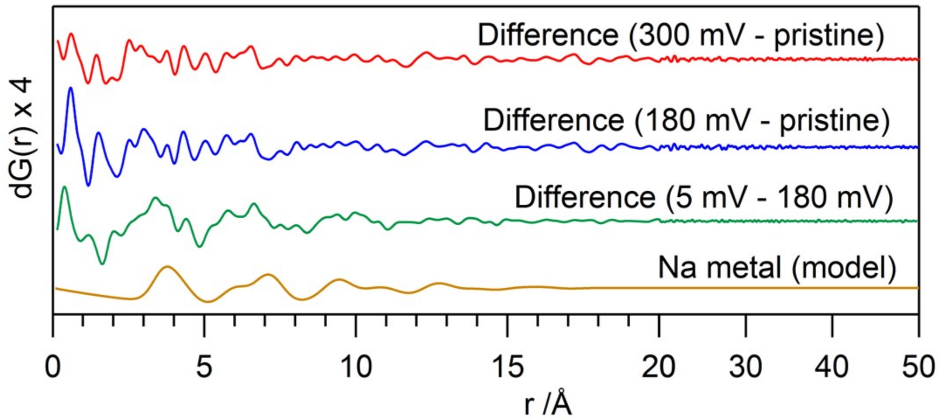

Figure S7: Difference PDFs for end of sodium insertion compared with the calculated PDF for sodium-metal. The PDF for sodium metal was calculated using PDFGui, with $U_{11} = U_{22} = U_{33} = 0.13$ and a spherical particle diameter of 20 Å.

5. Additional ex situ NMR spectra at different states of charge

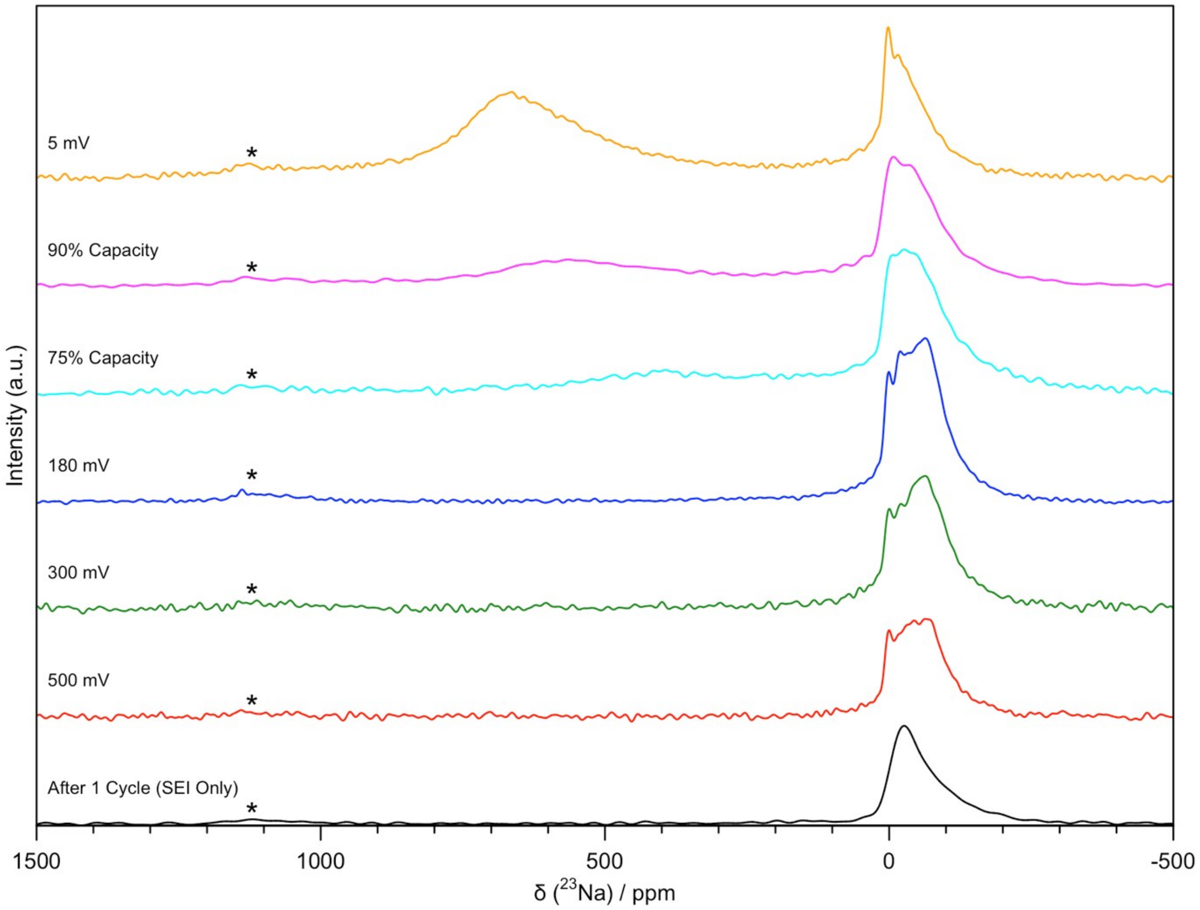

Figure S8: Additional *ex situ* ^{23}Na 60 kHz MAS NMR spectra of hard carbon anodes at various states of charge. Spinning sidebands are indicated with an asterisk (*). The black line corresponds to a spectrum after a complete discharge / charge cycle and represents the sodium that is irreversibly stored in the hard carbon. Intensities are normalised based upon the sample mass and the number of transients collected.

6. NMR spectra at different fields

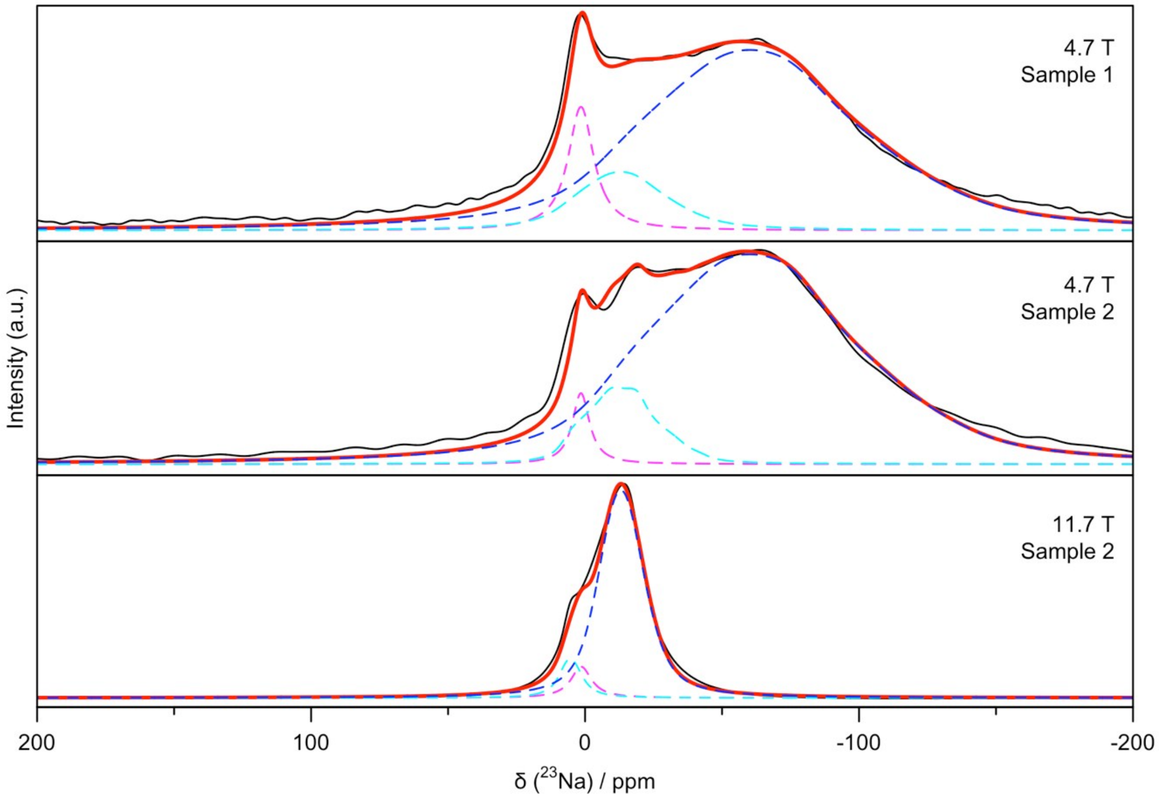

Figure S9: *Ex situ* ^{23}Na 60 kHz MAS NMR spectra of two different samples discharged to 180 mV and measured at magnetic fields of 4.7 T (samples 1 and 2) and 11.7 T (sample 2). Each spectrum was fit using the NMR parameters for 2nd order quadrupole coupling (central transition) in Bruker Topspin SOLA. A deconvolution of the spectra results in three peaks and is consistent with the influence of the magnetic field strength on the NMR signal line shape; the respective NMR coupling parameters are summarised in Table S2. Line broadening of 400 to 1800 Hz was applied to each signal to account for the breadth of each peak, resulting in the lack of the characteristic line shape features found in spectra of quadrupolar nuclei with large C_Q values. The magenta peak (peak 1) is assigned to residual electrolyte as its intensity was found to vary based on the electrode washing procedure performed (samples 1 and 2 at 4.7 T). The cyan peak (peak 2) is assigned to SEI as its intensity does not vary in a similar manner. Peak 3 (blue) corresponds to sodium reversibly stored within the hard carbon framework.

Table S3: Isotropic shift (δ_{iso}), quadrupolar coupling constant (C_Q), and asymmetry parameter of the quadrupole coupling (η_Q) for the three peaks used to deconvolute the spectra given in Figure S9.

	Peak 1 (Magenta)	**Peak 2 (Cyan)**	**Peak 3 (Blue)**
δ_{iso} / ppm	1.6	9.0	-4.0
C_Q / kHz	0	1500	2400
η_Q	0	0.6	0.6

References

1 M. Basham, J. Filik, M. T. Wharmby, P. C. Y. Chang, B. El Kassaby, M. Gerring, J. Aishima, K. Levik, B. C. A. Pulford, I. Sikharulidze, D. Sneddon, M. Webber, S. S. Dhesi, F. Maccherozzi, O. Svensson, S. Brockhauser, G. Náray and A. W. Ashton, *J. Synchrotron Radiat.*, 2015, **22**, 853–858.

2 X. Qiu, J. W. Thompson and S. J. L. Billinge, *J. Appl. Crystallogr.*, 2004, **37**, 678–678.

3 C. L. Farrow, P. Juhas, J. W. Liu, D. Bryndin, E. S. Božin, J. Bloch, T. Proffen and S. J. L. Billinge, *J. Phys. Condens. Matter*, 2007, **19**, 335219.

4 O. Pecher, P. M. Bayley, H. Liu, Z. Liu, N. M. Trease and C. P. Grey, *J. Magn. Reson.*, 2016, **265**, 200–209.

5 R. K. Harris and E. D. Becker, *J. Magn. Reson.*, 2002, **156**, 323–326.

6 M. Wojdyr, *J. Appl. Crystallogr.*, 2010, **43**, 1126–1128.

7 S. Hayashi and K. Hayamizu, *Bull. Chem. Soc. Jpn.*, 1989, 62, 2429–2430.